JCB

Supplemental material

Azoitei et al., **https://doi.org/10.1083/jcb.201812073**

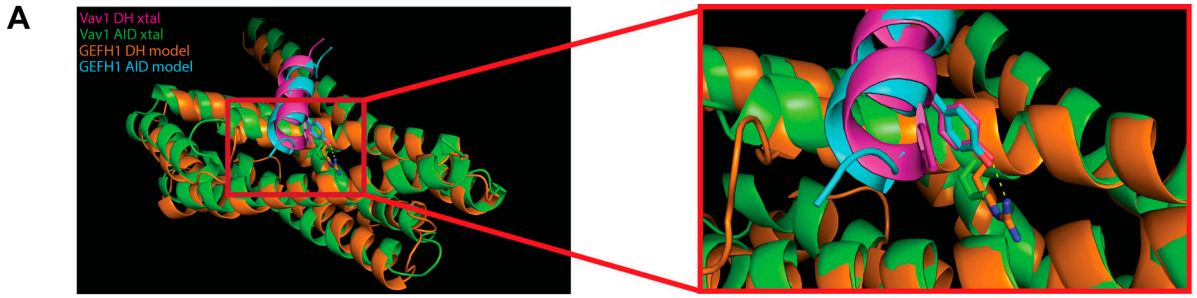

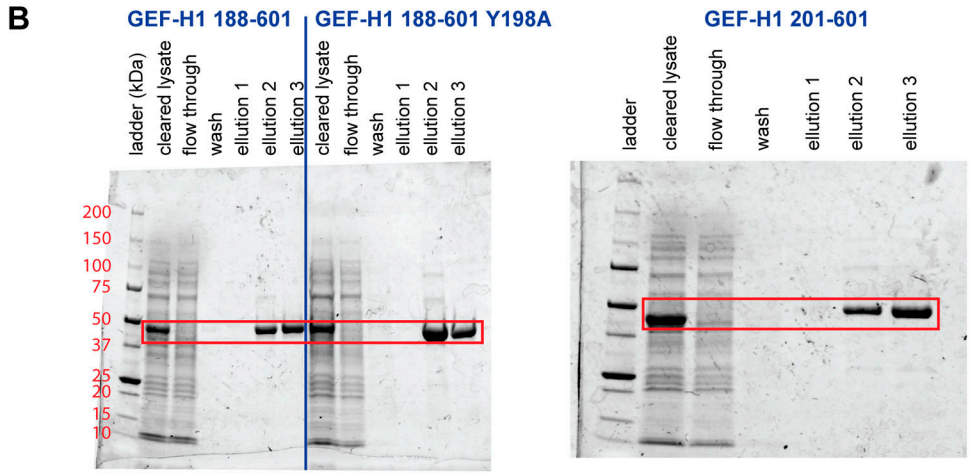

C

>GEF-H1 FLARE212

MSRIESLTRA RIDRSRELAS KTREKEKMKE AKDARYTNGH LFTTISVSGM TMCYACNKSI TAKEALICPT CNVTIHNRCK DTLANCTKVK QKQQKAALLK NNTALQSVSL RSKTTIRERP
SSAIYPSDSF RQSLLGSRRG RSSLSLAKSV STTNIAGHFN DESPLGLRRI LSQSTDSLNM RNRTLSVESL IDEAEVIYSE LMSDFEMDEK DFATGMVSKG EELFTGVVPI LVELDGDVNG
HKFSVSGEGE GDATYGKLTL KFICTTGKLP VPWPTLVTTL SWGVQCFARY PDHMKQHDFF KSAMPEGYVQ ERTIFFKDDG NYKTRAEVKF EGDTLVNRIE LKGIDFKEDG NILGHKLEYN
AIHGNVYITA DKQKNGIKAN FGLNCNIEDG SVQLADHYQQ NTPIGDGPVL LPDNHYLSTQ SKLSKDPNEK RDHMVLLEFV TAAGITLGMD ELYKSLTSGS GKPGSGEGST KGGSTSGSGK
PGSGEGSTKG GSTSGSGKPG SGEGSTKGGS TSGSGKPGSG EGSTKGGSAA AMVSKGEELF TGVVPILVEL DGDVNGHKFS VSGEGEGDAT YGKLTLKLLC TTGKLPVPWP TLVTTLGYGV
QCFARYPDHM KQHDFFKSAM PEGYVQERTI FFKDDGNYKT RAEVKFEGDT LVNRIELKGI DFKEDGNILG HKLEYNYNSH NVYIITADKQK NGIKANFKIR HNIEDGGVQL ADHYQQNTPI
GDGPVLLPDN HYLSYQSALF KDPNEKRDHM VLLEFLTAAG ITEGMDELYK SGADSWSLAV DSSFLQQHKK EVMKQQDVIY ELIQTELHHV RTLKIMTRLF RTGMLEELHL EPGVVQGLFP
CVDELSDIHT RFLSQLLERR RQALCPGSTR NFVIHRLGDL LISQFSGPSA EQMCKTYSEF CSRHSKALKL YKELYARDKR FQQFIRKVTR PAVLKRHGVQ ECILLVTQRI TKYPLLISRI
LQHSHGIEEE RQDLTTALGL VKELLSNVDE GIYQLEKGAR LQEIYNRMDP RAQTPVPGKG PFGREELLRR KLIHDGCLLW KTATGRFKDV LVLLMTDVLV FLQEKDQKYI FPTLDKPSVV
SLQNLIVRDI ANQEKGMFLI SAAPPEMYEV HTASRDDRST WIRVIQQSVR TCPSREDFPL IETEDEAYLR RIKMELQQKD RALVELLREK VGLFAEMTHF QAEEDGGSGM ALPTLPRGLF
RSESLESPRG ERLLQDAIRE VEGLKDLLVG PGVELLLTPR EPALPLEPDS GGNTSPGVTA NGEARTFNGS IELCRADSDS SQRDRNGNQL RSPQEEALQR LVNLYGLLHG LQAAVAQQDT
LMEARFPEGP ERREKLCRAN SRDGEAGRAG AAPVAPEKQA TELALLQRQH ALLQEELRRC RRLGEERATE AGSLEARLRE SEQARALLER EAEEARRQLA ALGQTEPLPA EAPWARRPVD
PRRRSLPAGD ALYLSFNPPQ PSRGTDRLDL PVTTRSVHRN FEDRERQELG SPEERLQDSS DPDTGSEEEG SSRLSPPHSP RDFTRMQDIP EETESRDGEA VASES

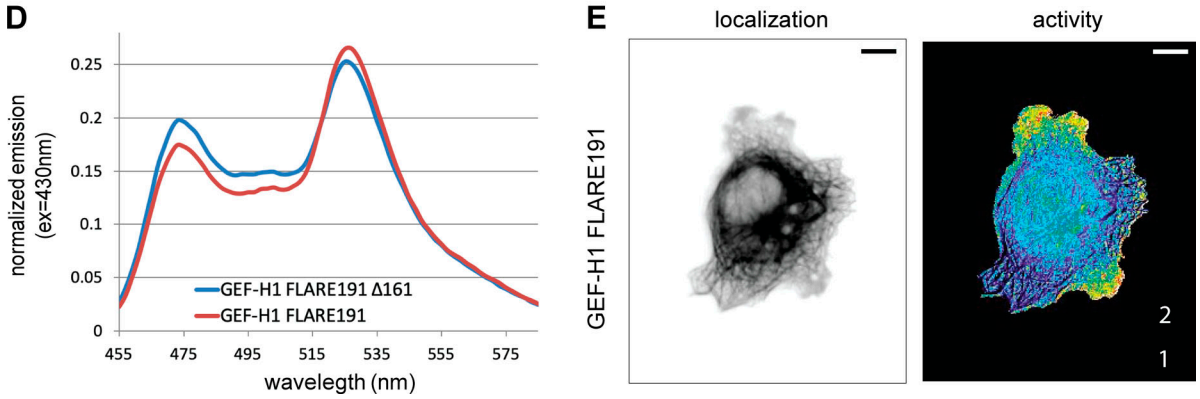

Figure S1. **GEF-H1 DH–AID interactions and biosensor design. (A)** Homology model of the GEF-H1 AID and DH domain interaction aligned on the known structure of Vav1 AID-DH complex (Protein Data Bank ID 3KY9; left). Complexes were aligned on the conserved regions 1 and 3 (CR1 and CR3) of their DH domains. Tyr198 of GEF-H1 recapitulates the key DH contact (dotted line) that Tyr174 of Vav1 forms (stick residues; right). **(B)** Purification of GEF-H1 constructs expressed recombinantly in *Escherichia coli*. Numbers indicated the subsequence included in the constructs (as referenced in UniProtKB entry Q92974-1). Constructs include the DH-PH domains and variable AIDs. **(C)** Amino acid sequence of GEF-H1 FLARE212 biosensor. **(D)** Emission spectra of unmodified and hyperactivated (Δ161) GEF-H1 FLARE191 expressed in suspended HEK293T cells (excitation at 405 nm). **(E)** Representative localization and activity map of GEF-H1 FLARE191 in COS-7 cells. Scale bar = 10 µm.

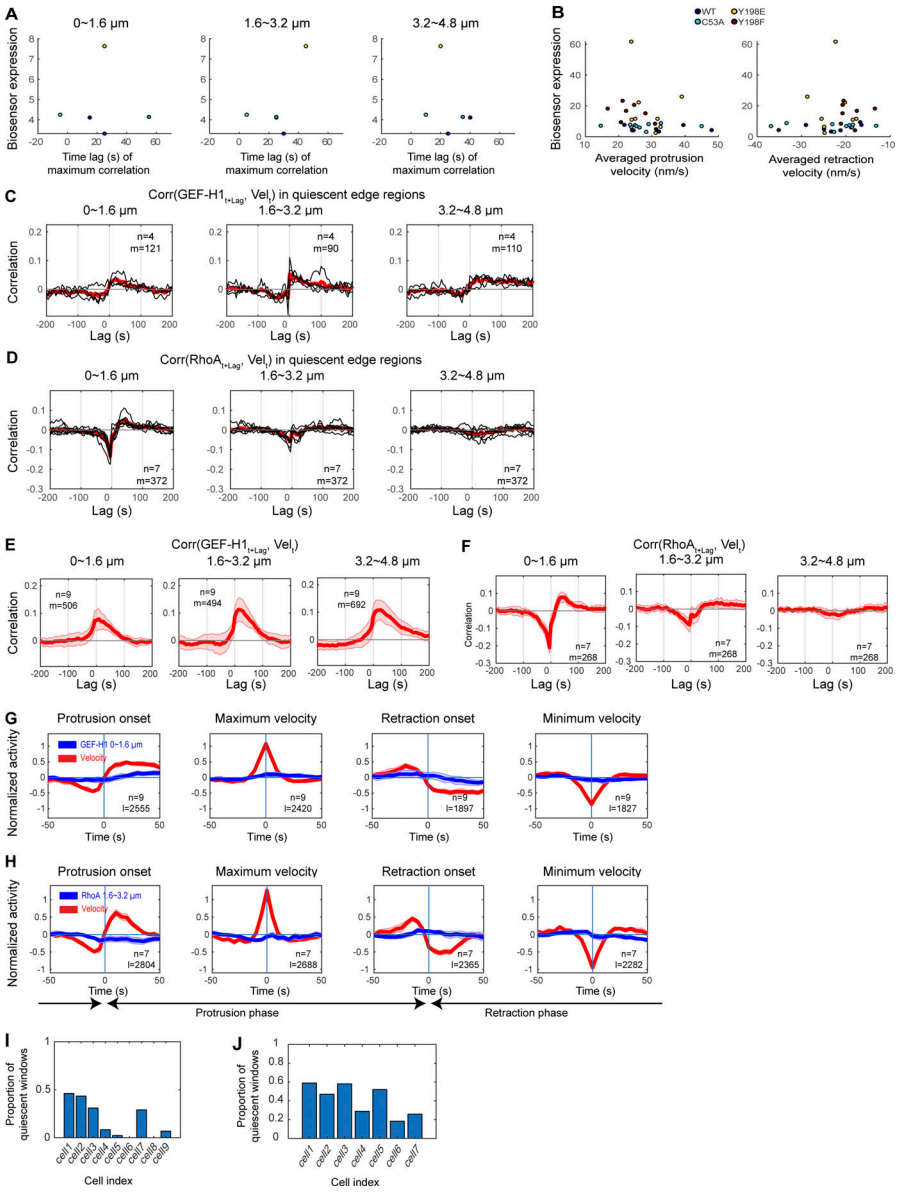

Figure S2. **Dynamics of GEF-H1 and RhoA activity relative to edge motions. (A and B)** GEF-H1 biosensor expression levels have no effects on cell edge motion and cross-correlations between the biosensor activity and edge velocity. **(A)** Relationship between relative biosensor expression levels and time lags of maximum correlation for individual cells (n = 5), at three different distances from the edge. The expression level has no significant Pearson's correlation with the time lag (r = 0.02, P = 0.98 at ~0–1.6 μm; r = 0.63, P = 0.26 at ~1.6–3.2 μm; r = −0.28, P = 0.65 at ~3.2–4.8 μm). **(B)** Relationship between biosensor expression level and averaged P/R velocities over individual cells and various mutants of biosensors. The expression level has no significant Pearson's correlation with edge motion (r = −0.18, P = 0.31 for protrusion velocity; r = 0.07, P = 0.69 for retraction velocity). Expression levels were determined relative to the fluorescence of the media in the shade-corrected donor image, a constant reference minimally susceptible to bleaching. **(C and D)** GEF-H1 (C) and RhoA (D) correlation curves obtained only from quiescent edge regions, exhibiting weaker coupling than the ones from nonquiescent regions shown in E and F below. Curves from individual cells are shown in black, with the average values shown in red. Four cells with enough quiescent edge regions shown below in I for GEF-H1 and J for RhoA are analyzed. **(E)** Averaged correlation curves between GEF-H1 biosensor activity and edge velocity. GEF-H1 exhibits significant positive correlations at positive lags, indicating edge protrusion precedes GEF-H1 activation. Maximum correlations are observed as 0.08/0.11/0.11 in the ~0–1.6-, ~1.6–3.2-, and ~3.2–4.8-μm regions, with a lag of 10/15/25 s at the three respective distance bands. Maximum edge velocity is followed by maximum GEF-H1 activity by 10–25 s. Correlation curves of individual cells (n = 9) are averaged (solid lines), and shaded confidence bands indicate ±2 × SEM displaying cell-to-cell variation. Quiescent fractions of the edge are excluded from the analysis through a statistical test (see Materials and methods), since such regions exhibit weaker or near-zero cross-correlations as shown in C. The total number of windows sampled (m) is indicated. **(F)** Averaged correlation curves between RhoA biosensor activity and edge velocity. RhoA activity exhibits significant negative correlations at negative lags in the ~0–3.2-μm region but not in the ~3.2–4.8-μm region, indicating that RhoA activation precedes edge retraction only within the region ~0–3.2 μm from the edge. The strongest correlations are observed as −0.21 (-0.09) in ~0–1.6 (~1.6–3.2) μm from the edge with the same lag of −5 s, showing that maximum RhoA activity is followed by the fastest retraction ~5 s later. Correlation curves of individual cells (n = 7) are averaged (solid lines), and shaded confidence bands indicate ±2 × SEM. The total number of windows sampled (m) is indicated. **(G and H)** Average GEF-H1 (G) and RhoA (H) activation profiles around four edge motion events in the indicated regions. Solid curves represent averages of n independent experiments, and shaded confidence bands indicate ±2 × SEM. The total number of edge motion events (l) sampled is indicated. **(I and J)** The proportion of quiescent and subsequently excluded windows in each GEF-H1 (I) and RhoA (J) biosensor expressing cell.

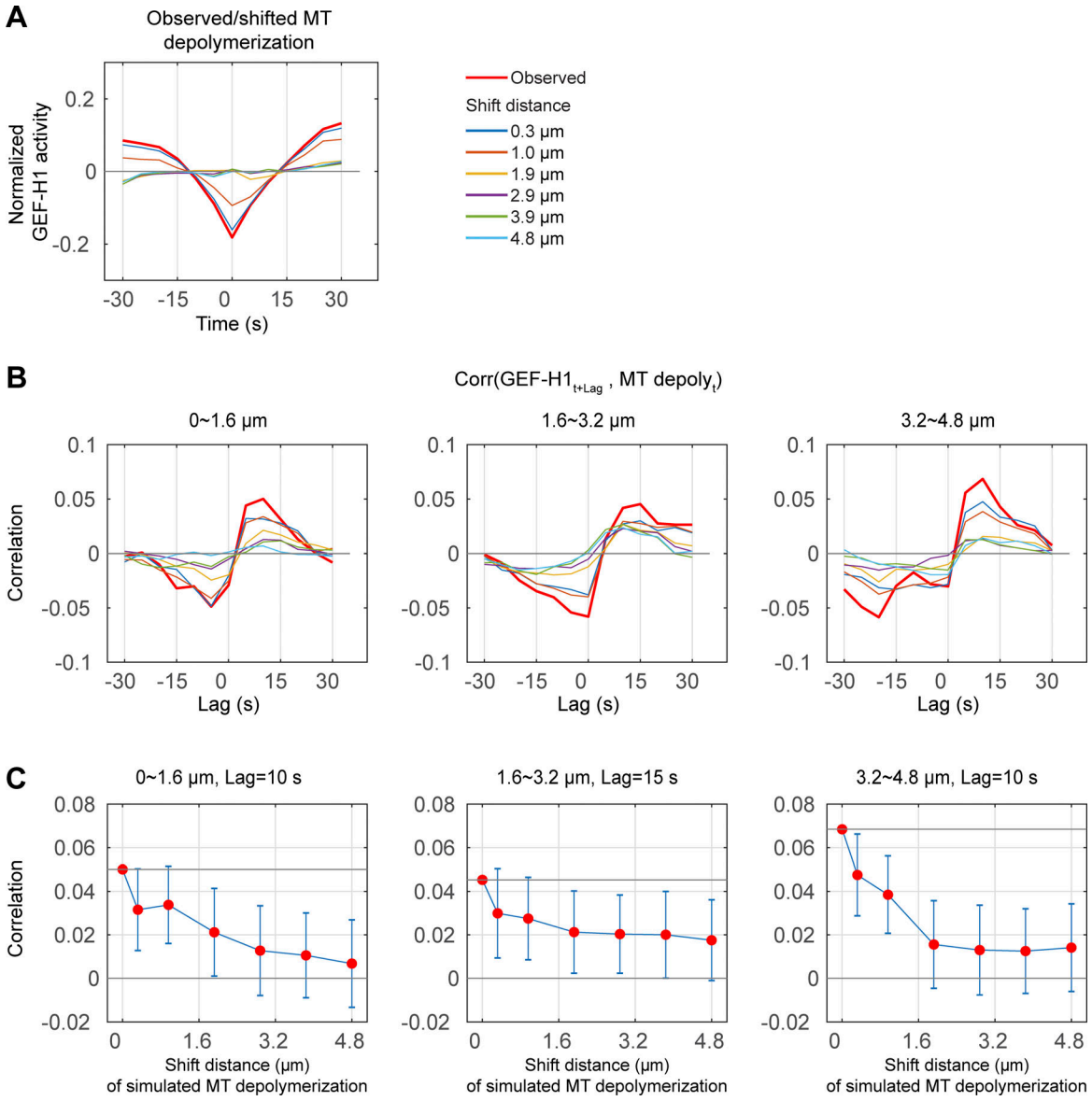

Figure S3. **Correlation of randomized MT depolymerization events and GEF-H1 activities. (A)** Fluctuation patterns of normalized local GEF-H1 activities before and after observed MT depolymerization events, and randomly shifted events over distances between 0 and 4.8 μm. The lowest GEF-H1 activity at the time of depolymerization decays toward zero as the shift distance increases. The fluctuation curves for shifted events are averages over 50 sets of spatial events. **(B)** Correlation curves between GEF-H1 activity and the occurrence rate of observed/shifted MT depolymerization at the three distances from the cell edge. Color labels are the same as in A. **(C)** The correlations at fixed lags diminish toward zero as the shift distance increases. Beyond 1.9-μm shifts, the shifted MT depolymerization events no longer correlate with GEF-H1 activity. Error bars indicate 95% confidence intervals obtained from the 50 sets of computations.

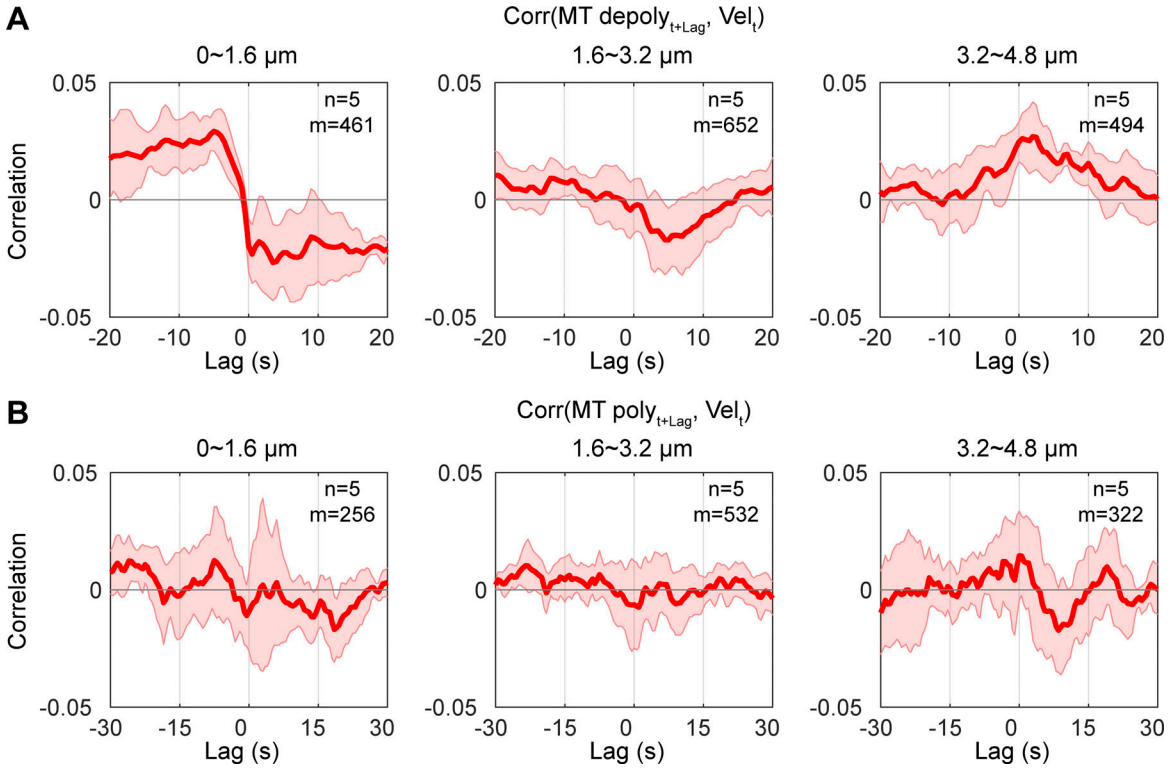

Figure S4. **MT dynamics show weak or no correlation with cell edge motion. (A and B)** Averaged correlation curves between edge velocity and instantaneous occurrence rate of MT depolymerization (A) and polymerization (B) at different distances from the edge. The correlations are measured using data from the EB3 channel acquired every 0.5 s. The occurrence rates of MT depolymerization are weakly correlated to edge motion (maximum correlations <0.03). Although the cross-correlations are weak, they suggest heterogeneous temporal coordination across different distances from the edge: maximum rates of MT depolymerization precede the fastest protrusions at ~0–1.6 μm, while the maximum depolymerization rates are synchronous with the fastest protrusions in the ~3.2–4.8-μm region (A). In contrast to MT depolymerization, the occurrence rates of MT polymerization events 2.5 s before depolymerization display no correlation with the edge motion shown in B.

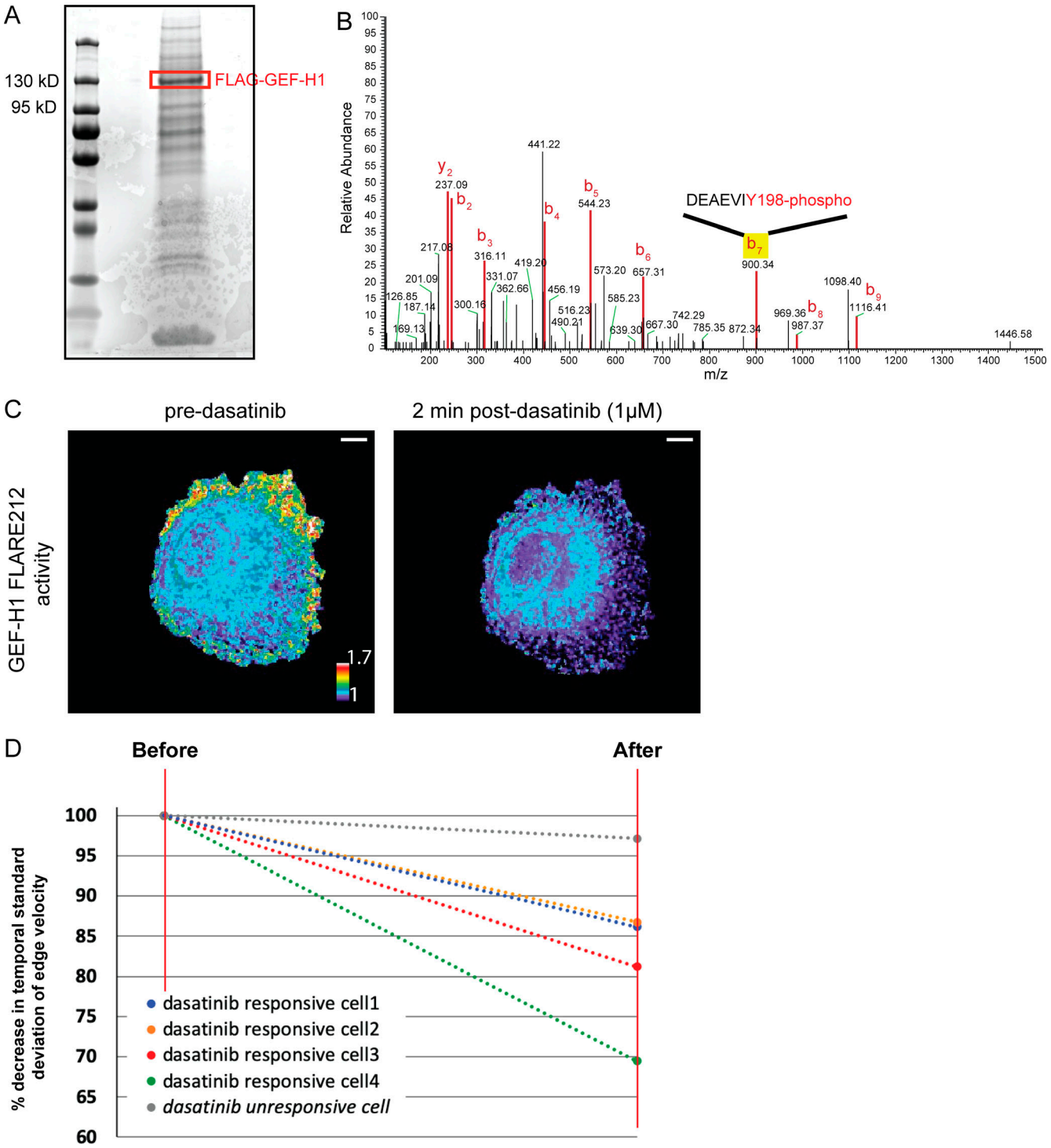

Figure S5. **The effect of GEF-H1 phosphorylation by Src. (A)** Coomassie-stained protein gel resulting from the immunoprecipitation of FLAG-GEF-H1 coexpressed with CA-Src in HEK293T cells. Red box indicates the band corresponding to FLAG-GEF-H1 (molecular weight = 115 kD). **(B)** AMS spectra of FLAG-GEF-H1, with the peak corresponding to DEAVIVY198-phospho peptides annotated. The b7 peak was missing from samples where FLAG-GEF-H1 was expressed alone (data not shown). **(C)** Activity distribution of GEF-H1 FLARE212 in MDA-MB-231 cells before and 2 min after treatment with 1 μM dasatinib. Scale bar = 10 μm. **(D)** Percent decrease in temporal SDs of edge velocity before and after dasatinib treatment in individual cells. Four cells exhibited a >10% decrease in the STD of velocity, indicating that low-dose dasatinib led to Src inhibition.

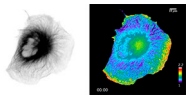

Video 1. **Localization (left) and activity map (right) of GEF-H1 FLARE212 in constitutively migrating COS-7 cells.** Duration: 30 min. 7 frames per second (FPS). Scale bar = 10 μm.

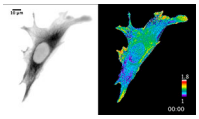

Video 2. **Treatment with nocodazole disrupts the MT network (right) and increases GEF-H1 FLARE212 activity (left) in motile MEFs.** Duration: 18 min. 7 FPS. Scale bar = 10 µm.

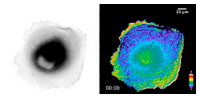

Video 3. **Localization (left) and activity map (right) of GEF-H1 FLARE212 in motile MDA-MB-231 cells.** Duration: 19.6 min.15 FPS. Scale bar = 10 µm.

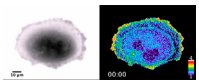

Video 4. **Localization (left) and activity map (right) of RhoA biosensor in motile MDA-MB-231 cells.** Duration: 12.9 min. 7 FPS. Scale bar = 10 µm.

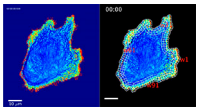

Video 5. **Cell edge tracking and cell frame of reference in an MDA-MB-231 cell expressing GEF-H1 FLARE212.** Left panel: Displacement vectors connecting two consecutive cell edges (red arrows, 7× original magnification) calculated by tracking edge motion. The displacements are averaged for every 1.6 µm (5 pixels) long-edge segments, determining the edge velocities shown in Fig. 3 B. Right panel: Sampling windows of ~1.6 × 1.6 μm^2 size partitioning the region 0–4.8 µm from the cell edge and tracking cell morphology. The tracked windows provide a morphodynamics-invariant coordinate system allowing us to measure subcellular GEF-H1 activities over time shown in Fig. 3 B. Duration: 500 s. Playback: 50×. Scale bar = 10 µm.

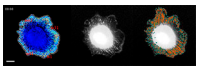

Video 6. **Reconstruction of MT growth in an MDA-MB-231 cell coexpressing GEF-H1 FLARE212 and EB3.** Left panel: GEF-H1 biosensor images acquired every 5 s and sampling windows following cell morphology. Middle panel: Computationally tracked plus-tips of growing MTs (red-yellow lines, slow-fast) in EB3 time-lapse images acquired every 0.5 s. Blue dots mark the ends of the trajectories. Right panel: All the trajectories and their ending events, which determine the MT depolymerization events shown in Figs. 4 and 5. Duration: 50 s. Playback: 7.5×. Scale bar = 10 µm.

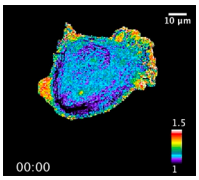

Video 7. **Inhibition of endogenous Src with a low dose of dasatinib (10 nM) leads to decreased GEF-H1 FLARE212 activity in motile MDA-MB-231 cells.** Duration: 10 min. 7 FPS. Scale bar = 10 µm.

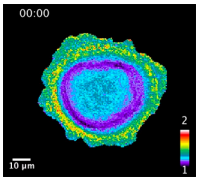

Video 8. **Localization (left) and activity map (right) of GEF-H1 FLARE212 Y198F biosensor mutant in motile MDA-MB-231 cells.** Duration: 15 min. 7 FPS. Scale bar = 10 µm.